Pis'ma v ZhETF, vol. 91, iss. 8, pp. 451 – 456 © 2010 April 25

Order parameter sign-reversal near $s_{\pm}$-superconductor surface

A. M. Bobkov, I. V. Bobkova[1)]

Institute of Solid State Physics, 142432 Chernogolovka, Moscow reg., Russia

Submitted 1 February 2010
Resubmitted 12 March 2010

The superconducting order parameter and LDOS spectra near an impenetrable surface are studied on the basis of selfconsistent calculations for a two band superconductor with nodeless extended s-wave order parameter symmetry, as possibly realized in Fe-based high-temperature superconductors. It is found that for a wide range of parameters the spatial behavior of the order parameter at a surface is not reduced to a trivial suppression. If the interband scattering at a surface is of the order of the intraband one or dominates it, it can be energetically favorable to change the symmetry of the superconducting state near the surface from $s_{\pm}$ to conventional s-wave. The range of existing of this surface conventional superconductivity is very sensitive to the relative values of interband and intraband pairing potentials. It is shown that the LDOS spectra near the surface can qualitatively differ upon calculating with and without taking into account the selfconsistency of the order parameter.

The discovery of a new family of iron-based high-temperature superconductors with distinct multi-orbital band structure [1 – 3] has renewed interest to the problem of multi-band superconductivity, firstly discussed fifty years ago [4, 5]. It was proposed theoretically [6, 7] that the Fe-based superconductors represent the first example of multigap superconductivity with a phase difference between the superconducting condensates belonging to different bands. This state was discussed previously [8, 9], but not yet observed in nature. In the most simple case there is the phase difference π between the superconducting condensates arising on the hole Fermi surfaces around Γ point and the electron Fermi surfaces around M point. This so-called $s_{\pm}$ (or extended s-wave) state has been favored by a variety of models within random phase approximation (RPA) [7, 10, 11] and renormalization group techniques [12 – 14]. Currently the $s_{\pm}$-state is viewed to be the most plausible candidate for the role of the superconducting order parameter in these compounds.

Surface and interface phenomena in $s_{\pm}$-superconductors have attracted considerable recent attention. The formation of bound states at a free surface of an $s_{\pm}$-superconductor [15 – 18], at an $S_{\pm}/N$ interface [19 – 22], an $N/S/S_{\pm}$ junction [23] and at Josephson junctions including $s_{\pm}$-superconductors [24, 22] was investigated theoretically. In particular, the finite energy subgap bound states (depending on the interface parameters) were found and their influence on the conductance spectra and Josephson current was investigated.

However almost all these calculations (except for a few numerical results [19]) assume non-selfconsistent superconducting order parameter (OP). In the present paper we focus on the study of the OP at a surface of $s_{\pm}$-superconductor. We have found that for a wide range of parameters the spatial behavior of the OP at a surface can not be reduced to a trivial suppression. If the interband scattering at a surface R_{12} is of the order of the intraband one R_0 or dominates it, it can be energetically favorable to change the symmetry of the superconducting state near the surface from $s_{\pm}$ to conventional s-wave. The range of existing of this surface conventional superconductivity is very sensitive to the relative values of interband and intraband pairing potentials. We demonstrate that the selfconsistent OP behavior affects the surface local density of states (LDOS) profiles, and, consequently, should be taking into account when interpreting experimental results. It is worth to note here that, while there is a wide parameter range of existing complex OP at the surface region [25], in this paper we only discuss the case when the surface OP is of conventional s-wave type.

We consider an impenetrable surface of a clean two-band superconductor. The OP is assumed to be of $s_{\pm}$-symmetry in the bulk of the superconductor, that is the phase difference between the OP's in the two bands (called 1 and 2) is π. It is supposed that an incoming quasiparticle from band 1,2 can be scattered by the surface as into the same band (intraband scattering), so as into the other band (interband scattering).

We make use of the quasiclassical theory of superconductivity, where all the relevant physical information is contained in the quasiclassical Green function $\hat{g}_i(\varepsilon, \mathbf{p}_f, x)$ for a given quasiparticle trajectory. Here ε is the quasiparticle energy measured from the chemical potential, $\mathbf{p}_f$ is the momentum on the Fermi surface

1)e-mail: bobkova@issp.ac.ru

(that can have several branches), corresponding to the considered trajectory, x is the spatial coordinate along the normal to the surface and $i = 1,2$ is the band index. Quasiclassical Green function is a 2×2 matrix in particle-hole space, that is denoted by the symbol $\hat{}$. The equation of motion for $\hat{g}_i(\varepsilon, \mathbf{p}_f, x)$ is the Eilenberger equation subject to the normalization condition [26, 27]. For superconductivity of $s_\pm$-type, when the pairing of electrons from different bands is absent, the Eilenberger equations corresponding to the bands 1 and 2 are independent. The trajectories belonging to the different bands can only be entangled by the surface, which enters the quasiclassical theory in the form of effective boundary conditions connecting the incident and outgoing trajectories.

However, owing to the normalization condition for the quasiclassical propagator, the boundary conditions for the quasiclassical Green functions are formulated as non-linear equations [28 – 30]. Furthermore, they contain unphysical, spurious solutions, so their practical use is limited. For this reason in the present work we make use of the quasiclassical formalism in term of so-called Riccati amplitudes [31, 32], that allows an explicit formulation of boundary conditions [32 – 36]. The retarded Green function $\hat{g}_i(\varepsilon, \mathbf{p}_f, x)$, which is enough for a complete description of an equilibrium system, can be parametrized via two Riccati amplitudes (coherence functions) $\gamma_i(\varepsilon, \mathbf{p}_f, x)$ and $\tilde{\gamma}_i(\varepsilon, \mathbf{p}_f, x)$ (in the present paper we follow the notations of Refs. [32, 36]). The coherence functions obey the Riccati-type transport equations. In the considered here case of two-band clean $s_\pm$-superconductor the equations for the two bands are independent and read as follows

$$iv_{ix}\partial_x \gamma_i + 2\varepsilon\gamma_i = -\Delta_i^* \gamma_i^2 - \Delta_i, \tag{1}$$

$$\tilde{\gamma}_i(\varepsilon, \mathbf{p}_f, x) = \gamma_i^*(-\varepsilon, -\mathbf{p}_f, x). \tag{2}$$

Here v_{ix} is the normal to the surface Fermi velocity component for the quasiparticle belonging to band i. Δ_i stands for the OP in the i-th band, which should be found self-consistently.

Let us suppose that the surface is located at $x = 0$ and the superconductor occupies the halfspace $x > 0$. For the sake of simplicity we assume that the surface is atomically clean and, consequently, conserves parallel momentum component. Then there are four quasiparticle trajectories, which are involved in each surface scattering event. These are two incoming trajectories belonging to the bands 1,2 (with $v_{ix} < 0$) and two outgoing ones (with $v_{ix} > 0$). It can be shown [32, 36] that the coherence function $\gamma_i(\varepsilon, \mathbf{p}_f, x)$, corresponding to the incoming trajectory can be unambiguously calculated making use of Eq. (1) up to the surface starting from its asymptotic value in the bulk

$$\gamma_i^b = -\frac{\Delta_i^b \mathrm{sgn}\varepsilon}{|\varepsilon| + \sqrt{(\varepsilon + i\delta)^2 - {\Delta_i^b}^2}}, \tag{3}$$

where Δ_i^b is the bulk value of the OP in the appropriate band, $\delta > 0$ is an infinitesimal. As for the coherence function $\tilde{\gamma}_i(\varepsilon, \mathbf{p}_f, x)$, it is determined unambiguously by the asymptotic conditions for the outgoing trajectories and can be obtained according to Eqs. (1),(2).

Otherwise, the coherence functions $\gamma_i(\varepsilon, \mathbf{p}_f, x)$ for the outgoing trajectories and, correspondingly, $\tilde{\gamma}_i(\varepsilon, \mathbf{p}_f, x)$ for the incoming ones should be calculated from Eq. (1) supplemented by the boundary conditions at the surface and Eq. (2). The surface is described by the normal state scattering matrix for particle-like excitations, denoted by S and for hole-like excitations, denoted by $\widetilde{S}$, that connect outgoing with incoming quasiparticles. The scattering matrix S have elements $S_{\mathbf{k}_i \mathbf{p}_j}$, which connect outgoing quasiparticles from band i with momentum $\mathbf{k}_i$ to the incoming ones belonging to band j with momentum $\mathbf{p}_j$. Here and below all the momenta corresponding to the incoming trajectories are denoted by letter $\mathbf{p}$ and all the momenta for the outgoing quasiparticles are denoted by $\mathbf{k}$. For the model we consider S is a 2×2-matrix (for the particular value of the momentum parallel to the surface) in the trajectory space. It obeys the unitary condition $SS^\dagger = 1$ and without loss of generality can be parameterized by three quantities R_{12}, Θ and α as follows

$$\begin{pmatrix} S_{\mathbf{k}_1\mathbf{p}_1} & S_{\mathbf{k}_1\mathbf{p}_2} \\ S_{\mathbf{k}_2\mathbf{p}_1} & S_{\mathbf{k}_2\mathbf{p}_2} \end{pmatrix} = \begin{pmatrix} \sqrt{R}_0 e^{i\Theta} & i\alpha\sqrt{R_{12}} \\ i\alpha\sqrt{R_{12}} & \sqrt{R}_0 e^{-i\Theta} \end{pmatrix}, \tag{4}$$

where R_0 and R_{12} are coefficients of intraband and interband reflection, respectively. They obey the constraint $R_0 + R_{12} = 1$. The phase factors $\alpha = \pm 1$ and Θ appear to be unimportant for further consideration. While in general the scattering matrix elements are functions of the momentum parallel to the surface $\mathbf{p}_{||}$, we disregard this dependence in order to simplify the analysis. The scattering matrix $\widetilde{S}$ for hole-like excitations are connected to S by the relation $\widetilde{S}(\mathbf{p}_{||}) = S^{tr}(-\mathbf{p}_{||})$. In the absence of spin-orbit interaction the S-matrix elements are only functions of $|\mathbf{p}_{||}|$, that is in the case we consider $\widetilde{S} = S$.

From the general boundary conditions [36], which are also valid for a multiband system, one can obtain the explicit values of the coherence functions $\gamma_i(\varepsilon, \mathbf{k}, x = 0)$

and $\tilde{\gamma}_i(\varepsilon, \mathbf{p}, x = 0)$ via the scattering matrix elements and the values of the coherence functions $\gamma_i(\varepsilon, \mathbf{p}, x = 0)$ and $\tilde{\gamma}_i(\varepsilon, \mathbf{k}, x = 0)$ at the surface. They read as follows

$$\gamma_{1\mathbf{k}} = R_0\gamma_{1\mathbf{p}} + R_{12}\gamma_{2\mathbf{p}} - \frac{R_0 R_{12}\tilde{\gamma}_{2\mathbf{k}}(\gamma_{1\mathbf{p}} - \gamma_{2\mathbf{p}})^2}{1 + \tilde{\gamma}_{2\mathbf{k}}\left(R_{12}\gamma_{1\mathbf{p}} + R_0\gamma_{2\mathbf{p}}\right)}, \tag{5}$$

$$\tilde{\gamma}_{1\mathbf{p}} = R_0\tilde{\gamma}_{1\mathbf{k}} + R_{12}\tilde{\gamma}_{2\mathbf{k}} - \frac{R_0 R_{12}\gamma_{2\mathbf{p}}(\tilde{\gamma}_{1\mathbf{k}} - \tilde{\gamma}_{2\mathbf{k}})^2}{1 + \gamma_{2\mathbf{p}}\left(R_{12}\tilde{\gamma}_{1\mathbf{k}} + R_0\tilde{\gamma}_{2\mathbf{k}}\right)}. \tag{6}$$

Here the arguments $(\varepsilon, x = 0)$ of all the coherence functions are omitted for brevity, $\gamma_{i\mathbf{p}} \equiv \gamma_i(\mathbf{p})$ and $\tilde{\gamma}_{i\mathbf{p}} \equiv \tilde{\gamma}_i(\mathbf{p})$ and the analogous notations are used for $\gamma_i(\mathbf{k})$ and $\tilde{\gamma}_i(\mathbf{k})$. Quantities $\gamma_{i\mathbf{p}}$ and $\tilde{\gamma}_{i\mathbf{k}}$, entering Eqs. (5) and (6) are to be calculated from Eqs. (1) and (2) supplemented by the appropriate asymptotic condition. The coherence functions $\gamma_{2\mathbf{k}}$ and $\tilde{\gamma}_{2\mathbf{p}}$ are obtained by the interchanging $1 \leftrightarrow 2$ in all the coherence function band indices at the right-hand side of Eqs. (5) and (6), respectively.

Now, substituting the coherence functions into the self-consistency equation

$$\Delta_i(x) = -T\sum_{\varepsilon_n, j}\lambda_{ij}\left\langle\frac{-2i\pi\gamma_{j\mathbf{p}_f}}{1 + \gamma_{j\mathbf{p}_f}\tilde{\gamma}_{j\mathbf{p}_f}}\right\rangle_{\mathbf{p}_f}, \tag{7}$$

we iterate system (1)–(3), (5)–(7) until it converges. In Eq. (7) $\lambda_{ii} < 0$ is the dimensionless pairing potential for band i and $\lambda_{12} = \lambda_{21}$ is the dimensionless interband pair-scattering potential. We choose $\lambda_{12} > 0$, which stabilizes $s_\pm$ OP in the bulk. The Matsubara frequencies ε_n enter the coherence functions via the substitution $\varepsilon + i\delta \to i\varepsilon_n$. $\langle ... \rangle_{\mathbf{p}_f}$ means the anomalous Green function averaged over the entire Fermi surface, that is $\mathbf{p}_f$ incorporates as the incoming trajectories $\mathbf{p}$, so as the outgoing ones $\mathbf{k}$. For concreteness we suppose the Fermi surface to be cylindrical for the each band. However, our results do not qualitatively sensitive to this assumption.

The spatial profiles of the OP calculated according to the described above technique, are represented in Figs.1–3. We assume that in the bulk $|\Delta_1^b| > |\Delta_2^b|$. Panels (a) of Figs.1–3 demonstrate the spatial OP profiles for band 1, while panels (b) correspond to band 2.

Fig.1 shows the dependence of the effect on the interband pair-scattering value λ_{12}. While the larger OP (in band 1) is simply suppressed near the surface and the magnitude of the suppression is only slightly sensitive to λ_{12} (at least, in the range we consider), the smaller OP (in band 2) reverses its sign near the surface. Thus, there is a surface region, which size is comparable to the superconducting coherence length ξ, where

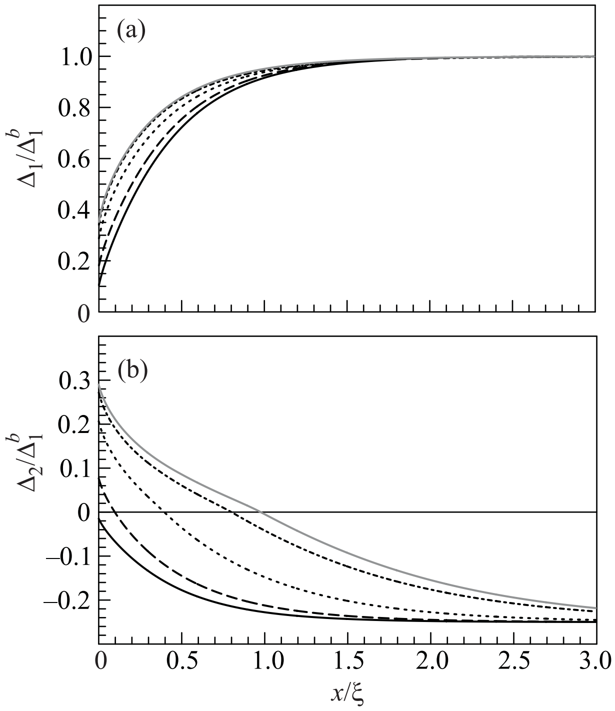

Fig.1. Spatial profiles of the OP corresponding to band 1 (panel(a)) and band 2 (panel(b)) near the surface ($x = 0$) for different values of interband pair scattering. $R_{12} = 1$, $\Delta_2^b = -0.25\Delta_1^b$, temperature $T = 0.3\Delta_1^b$. The values of intraband pairing potentials λ_{ii} are adjusted to keep Δ_1^b and Δ_2^b unchanged upon varying λ_{12}. The particular values of coupling constants are the following: $(\lambda_{12}, \lambda_{11}, \lambda_{22}) = (0.06, -0.2607, -0.0327)$ for black solid curve, $(0.03, -0.2695, -0.1353)$ for dashed curve, $(0.01, -0.2753, -0.2036)$ for dotted curve, $(0.004, -0.2771, -0.2241)$ for dashed-dotted curve and $(0.002, -0.2777, -0.2310)$ for gray solid curve. The superconducting coherence length $\xi = v_{1f}/\Delta_1^b$

$s_\pm$-superconductivity is superseded by the conventional one. The reason for this OP sign reversal is the interband surface scattering R_{12}, because it is energetically more favorable to minimize the OP gradient term along the quasiparticle trajectory. It is worth to note here somewhat similar effect of the OP sign reversal for the smaller gap due to magnetic impurities [8].

Fig.1 demonstrates that the weaker the interband pair scattering potential the wider the region, where the conventional s-wave superconductivy exists. It can be qualitatively understood on the basis of the self-consistency equation (7): the phase of the smaller OP is determined to a great extent by the phase of the dominant OP via the term λ_{12}. The weaker this connection the less energy cost to reverse the phase. As it is seen from the caption to Fig.1, in the particular calculations we take $|\lambda_{12}| \ll |\lambda_{11}|$. Such a choice of parameters is

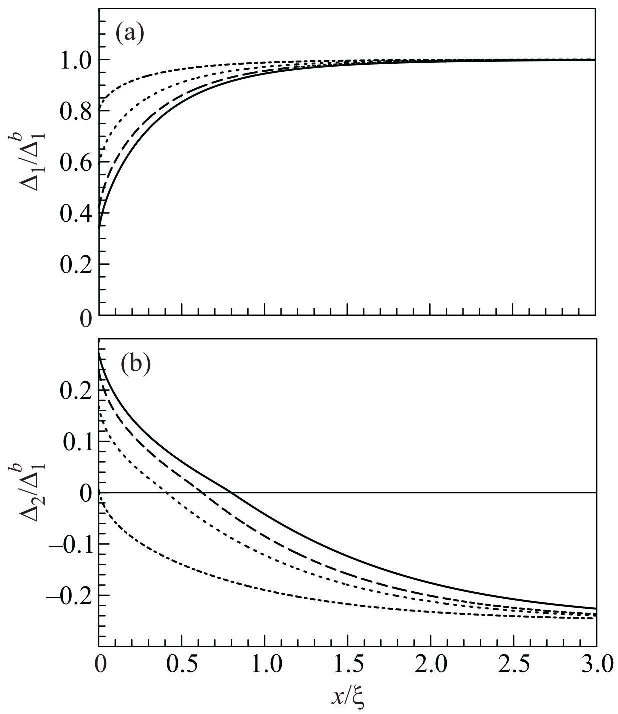

Fig.2. Spatial profiles of the OP near the surface in band 1 (panel (a)) and in band 2 (panel (b)) for different values of interband surface scattering R_{12}. $\Delta_2^b = -0.25\Delta_1^b$, $T = 0.3\Delta_1^b$, $(\lambda_{12}, \lambda_{11}, \lambda_{22}) = (0.004, -0.2771, -0.2241)$. $R_{12} = 1$ for black solid curve, 0.8 for dashed curve, 0.5 for dotted curve and 0.2 for dashed-dotted curve

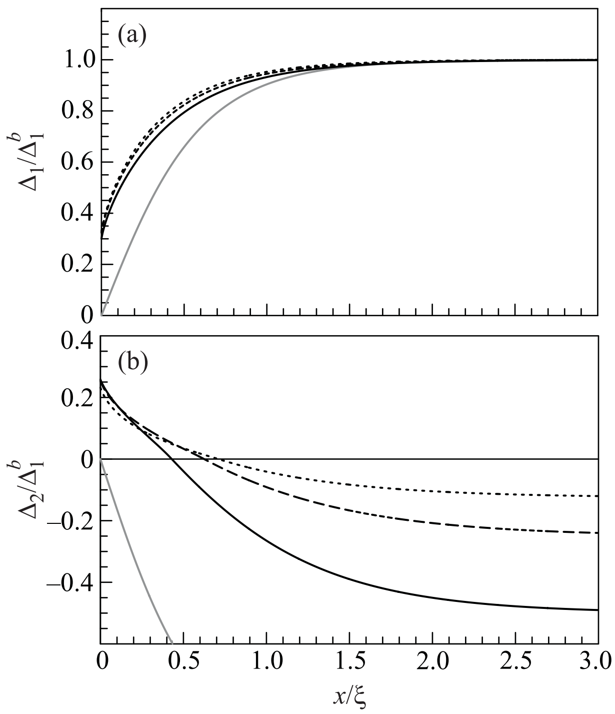

Fig.3. Spatial profiles of the OP near the surface in band 1 (panel (a)) and in band 2 (panel (b)) for different values of the ratio Δ_2^b/Δ_1^b. $T = 0.3\Delta_1^b$, $\lambda_{12} = 0.005$, $R_{12} = 1$. $\Delta_2^b/\Delta_1^b = -1$ ($\lambda_{11} = \lambda_{22} = 0.2732$) for gray solid curve, $\Delta_2^b/\Delta_1^b = -0.5$ ($\lambda_{11} = 0.2754, \lambda_{22} = 0.2393$) for black solid curve, $\Delta_2^b/\Delta_1^b = -0.25$ ($\lambda_{11} = 0.2768, \lambda_{22} = 0.2207$) for dashed curve and $\Delta_2^b/\Delta_1^b = -0.125$ ($\lambda_{11} = 0.2775, \lambda_{22} = 0.2011$) for dotted curve

consistent with the experimental estimates of the coupling constants for FeSe [37].

The curves represented in Fig.1 are calculated under the assumption of purely interband surface scattering $R_{12} = 1$, when the OP sign reversal is strongest. In order to investigate the effect in the more realistic situation one needs to take into account intraband scattering R_0. The corresponding results are demonstrated in Fig.2. It is seen that the region of reversed OP existence shrinks with increasing of R_0. However the effect remains to be pronounced even if the portion of intraband scattering exceeds 50%. Thus, we believe that the self-consistent OP treatment is essential for polycrystalline samples, for example, upon analysing spectroscopic data.

The considerable region of conventional s-wave surface superconductivity can only occur if the bulk OP's in the two bands essentially differ in magnitude. In case if $|\Delta_2^b|$ approaches to $|\Delta_1^b|$, the OP phase reversal region shrinks and, finally, the surface OP behavior reduces to the trivial suppression for the two bands if $|\Delta_1^b| = |\Delta_2^b|$. Otherwise, upon decreasing the ratio $|\Delta_2^b|/|\Delta_1^b|$ the surface region gets wider until its width saturates at some value of the ratio ($\sim 1/4$ for the considered case). This is illustrated in Fig.3.

Now we discuss how the described above OP spatial behavior affects LDOS near the surface. LDOS ρ_i corresponding to band i is calculated via the coherence functions as follows

$$\rho_i(x, \varepsilon) = \mathrm{Re} \left\langle \frac{1 - \gamma_{i\mathbf{p}_f} \tilde{\gamma}_{i\mathbf{p}_f}}{1 + \gamma_{i\mathbf{p}_f} \tilde{\gamma}_{i\mathbf{p}_f}} \right\rangle_{\mathbf{p}_f} . \qquad (8)$$

Figs.4 and 5 represent the LDOS at the surface ($x = 0$) as a function of quasiparticle energy. Left and right columns of the Figures demonstrate the LDOS for bands 1 and 2 separately. Upper row of each Figure shows LDOS plots, calculated taking into account the selfconsistent OP behavior. It should be compared to the lower row, where LDOS is plotted for the same parameters, but for the non-selfconsistent OP equal to its bulk value. The results represented in Fig.4 correspond to $R_{12} = 0.5$, while Fig.5 illustrates the case of purely interband scattering $R_{12} = 1$.

As it was already discussed in the literature, if $R_{12} \neq 0$ there are surface bound states in the system,

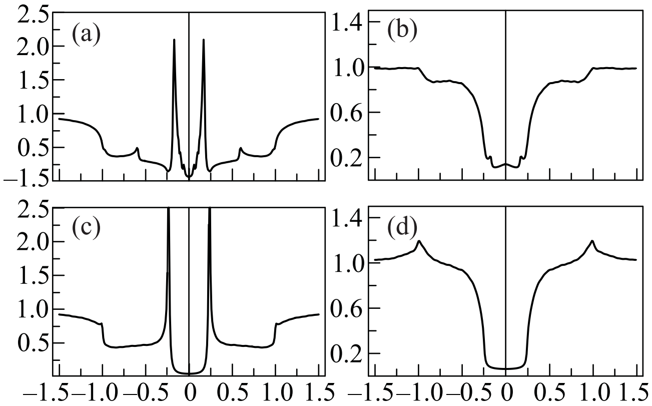

Fig.4. LDOS as a function of quasiparticle energy calculated at $x = 0$. The energy is measured in units of Δ_1^b. Left column represents LDOS for band 1, while right column corresponds to band 2. Upper row demonstrates the results of selfconsistent calculations and lower one shows the LDOS assuming non-selfconsistent OP. $(\lambda_{12}, \lambda_{11}, \lambda_{22}) = (0.004, -0.2771, -0.2241)$, $\Delta_2^b = -0.25\Delta_1^b$, $T = 0.3\Delta_1^b$, $R_{12} = 0.5$

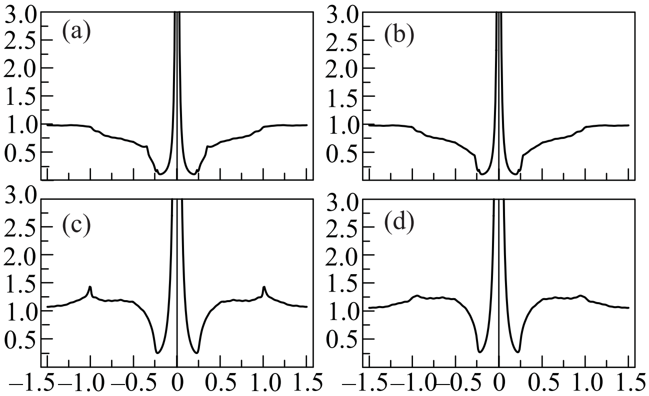

Fig.5. The same as in Fig.4, but corresponding to $R_{12} = 1$

which manifest themselves as well-pronounced peaks in the LDOS. At $R_{12} \to 1$ the bound state energies tend to zero, what can be clearly seen from the corresponding LDOS plots. For this case the LDOS is dominated by very strong zero-energy peak and the differences between selfconsistent and non-selfconsistent plots are not qualitative. It can be only noted that the features corresponding to gap edges (clearly seen at least in panel (c) of Fig.5) are washed out under selfconsistent calculation. At the same time for the intermediate value of interband scattering there are qualitative differencies between selfconsistent and non-selfconsistent results (see Fig.4). They can be summarize as follows: (i) while in the non-selfconsistent picture the bound state peaks are divided by the clearly defined gap, selfconsistency results in transforming this inner gap into "V"-shaped behavior, which is known to be more typical for the superconductors with OP nodes at the Fermi surface. We believe that this observation can be essential for interpreting experimental data. (ii) additional features (small peaks) appear in the subgap region upon taking into account selfconsistency. It is worth to note here that, in contrast to the interface OP behavior, the shape of LDOS profiles can be quite sensitive to the details of the microscopic model describing the interface, in particular to the concrete dependence of the scattering matrix elements on $\mathbf{p}_{||}$. However, if the particular microscopic scattering matrix model leads to the existence of an inner gap in the LDOS, it is inevitably transformed into "V"-shaped behavior under selfconsistent calculation, as it is demonstrated above. This fact is a consequence of spatial line of OP nodes appearing if the OP sign reversal takes place at the surface.

In summary, for a two band $s_{\pm}$-superconductor we have theoretically investigated the behavior of the OP at a specular reflecting surface. It is found that if the interband surface scattering is of the order of the intraband one or dominates it, the OP belonging to the band with smaller OP absolute value in the bulk reverses its sign at a surface region, thus giving rise to conventional s-wave surface superconductivity. This region of reversal sign OP is maximal for purely interband surface scattering and shrinks upon its diminishing. The effect is quite sensitive to the ratio between intraband and interband superconducting coupling constants and is more pronounced for smaller interband coupling constant. It is also shown that if the OP sign reversal takes place, it results in qualitative changes in the LDOS spectra near the surface.

The support by RFBR Grant # 09-02-00779 and the programs of Physical Science Division of RAS is acknowledged. A.M.B. was also supported by the Russian Science Support Foundation.

1. E. M. Brüning, C. Krellner, M. Baenitz et al., Phys. Rev. Lett. **101**, 117206 (2008).
2. J. Zhao, Q. Huang, C. de la Cruz et al., Nat. Mat. **7**, 953 (2008).
3. L. Pourovskii, V. Vildosola, S. Biermann, and A. Georges, Europhys. Lett. **84**, 37006 (2008).
4. H. Suhl, B. T. Matthias, and L. R.Walker, Phys. Rev. Lett. **3**, 552 (1959).
5. V. A. Moskalenko, Fiz. Met. Metalloved. **8**, 503 (1959) [Phys. Met. Metallogr. **8**, 25 (1959)].
6. I. I. Mazin, D. J. Singh, M. D. Johannes, and M. H. Du, Phys. Rev. Lett. **101**, 057003 (2008).
7. K. Kuroki, S. Onari, R. Arita et al., Phys. Rev. Lett. **101**, 087004 (2008).

8. A. A. Golubov and I. I. Mazin, Phys. Rev B **55**, 15146 (1997).
9. D. F. Agterberg, V. Barzykin, and L. P. Gorikov, Phys. Rev. B **60**, 14868 (1999).
10. V. Cvetković and Z. Tešanović, Europhys. Lett. **85**, 37002 (2009).
11. S. Graser, T. A. Maier, P. J. Hirschfeld, and D. J. Scalapino, New J. Phys. **11**, 025016 (2009).
12. A. V. Chubukov, D. Efremov, and I. Eremin, Phys. Rev. B **78**, 134512 (2008).
13. Fa Wang, H. Zhai, Y. Ran et al., Phys. Rev. Lett. **102**, 047005 (2009).
14. V. Cvetković and Z. Tešanović, Phys. Rev. B **80**, 024512 (2009).
15. P. Ghaemi, F. Wang, and A. Vishwanath, Phys. Rev. Lett. **102**, 157002 (2009).
16. Y. Nagai and N. Hayashi, Phys. Rev. B **79**, 224508 (2009).
17. S. Onari and Y. Tanaka, Phys. Rev. B **79**, 174526 (2009).
18. Y. Nagai, N. Hayashi, and M. Machida, arXiv:0910.4040.
19. H. Y. Choi and Y. Bang, arXrv:0807.4604.
20. J. Linder and A. Sudbo, Phys. Rev. B **79**, 020501(R) (2009).
21. A. A. Golubov, A. Brinkman, Y. Tanaka et al., Phys. Rev. Lett. **103**, 077003 (2009).
22. I. B. Sperstad, J. Linder, and A. Sudbo, Phys. Rev. B **80**, 144507 (2009).
23. X. Y. Feng and T. K. Ng, Phys. Rev B **79**, 184503 (2009).
24. W. F. Tsai, D. X. Yao, B. A. Bernevig, and J. P. Hu, Phys. Rev. B **80**, 012511 (2009).
25. A. M. Bobkov and I. V. Bobkova, in preparation.
26. A. I. Larkin and Y. N. Ovchinnikov, Zh. Eksp. Teor. Fiz. **55**, 2262 (1968) [Sov. Phys. JETP **28**, 1200 (1969)].
27. G. Eilenberger, Z. Phys. **214**, 195 (1968).
28. A. L. Shelankov, Sov. Phys. Solid State **26**, 981 (1984) [Fiz. Tved. Tela **26**, 1615 (1984)].
29. A. V. Zaitsev, Zh. Eksp. Teor. Fiz. **59**, 1015 (1984) [Sov. Phys. JETP **59**, 1015 (1984)].
30. A. Millis, D. Rainer, and J. A. Sauls, Phys. Rev. B **38**, 4504 (1988).
31. A. L. Shelankov, Sov. Phys. JETP **51**, 1186 (1980); A. L. Shelankov, J. Low Temp. Phys. **60**, 29 (1985).
32. M. Eschrig, Phys. Rev. B **61**, 9061 (2000).
33. A. Shelankov and M. Ozana, Phys. Rev. B **61**, 7077 (2000); A. Shelankov and M. Ozana, J. Low Temp. Phys. **124**, 223 (2001).
34. M. Fogelström, Phys. Rev. B **62**, 11812 (2000).
35. E. Zhao, T. Löfwander, and J.A. Sauls, Phys. Rev. B **70**, 134510 (2004).
36. M. Eschrig, Phys. Rev. B **80**, 134511 (2009).
37. R. Khasanov, M. Bendele, A. Amato et al., arXiv:0912.0471.